Shock accelerated cylindrical gas inhomogeneities
Part 2. A heavy gas cylinder

By J.W. Jacobs†

California Institute of Technology. Pasadena, CA 91125

Experiments have been carried out in which a cylindrical volume of a heavy gas is impulsively accelerated by a weak shock wave. A laminar jet of sulphur hexafluoride (SF_6) is used to produce the heavy gas cylinder. Planar laser induced fluorescence (PLIF) is used to visualize the flow. In viewing the PLIF images it is discovered that the vorticity that early on resides on the boundary between the two gasses, separates from the cylinder to form a pair of vortices. Subsequently these vortices wrap the heavy gas around them. This process is quite different from what is observed when the cylinder is lighter than its surroundings. Similar experiments with helium (Part 1 of this series) showed that a small amount light gas stays with the vorticity, eventually becoming part of the vortex cores. A simple model capable of explaining these differences is presented. In addition, the displacement of the jet cross section is measured and agrees reasonably well with previous experimental and computational results.

---

1. Introduction

Flows produced by the interaction of pressure and density gradients encompass a large class of problems in fluid mechanics. It is well known that the misalignment of pressure and density gradients produces vorticity, and thus motion, in an otherwise quiescent fluid. Generally, the magnitudes of the pressure gradients involved in these situations are small. Thus, for the most part these are relatively slow moving flows. For example in natural convection, motion is

---

† Present address: Department of Aerospace and Mechanical Engineering. University of Arizona. Tucson, AZ 85721

produced by the interaction of a density gradient caused by a nonuniform temperature distribution and a hydrostatic pressure gradient. Most often the temperature gradients are not large enough to produce a high degree of stratification. Even in cases where large density differences exist, the velocity of motion is often limited by a pressure gradient that results from gravity. On the other hand, even weak shock waves contain substantial pressure gradients. Thus, the interaction of a moderate density gradient with a weak shock wave produces a flow having considerable velocity.

This class of flows was first studied in the configuration of a nearly plane interface, separating gases of different density, by Richtmyer (1960) and Meshkov (1969). It was found that a small disturbance on the nearly flat interface will grow with time, when acted on by a passing shock wave. Rudinger & Somers (1960) later studied the interaction of plane shock waves with three-dimensional light and heavy gas inhomogeneities produced using either spark discharges or small jets of H_2, He or SF_6. This work was carried to more fundamental level by Haas & Sturtevant (1987) with experiments which studied the interaction of shock waves with light and heavy gas inhomogeneities having either cylindrical or spherical geometry. Since then Picone & Boris (1988) and others have worked to computationally reproduce the results of Haas & Sturtevant .

Part 1 of this series examined the flow produced by the interaction of a weak shock wave with a cylindrical region of gas that is lighter than its surroundings. This work improved on shortcomings in the earlier experimental investigations of Rudinger & Somers (1960) and Haas & Sturtevant (1987) by utilizing two new techniques. First, a technique was developed to produce light gas cylinders. A laminar jet was used to produce cylinders that were free from the membrane needed by Haas & Sturtevant to contain the light gas. Second, planar laser induced fluorescence (PLIF) was implemented to visualize the flow. The Helium flow was seeded with a small amount of the biacetyl (Epstein 1977), and then made to fluoresce with a sheet if laser light.

The experiments in this part of the series utilize the same techniques used in Part 1. Thus these experiments benefit from the improvements of Part 1 over previous experiments. Sulphur hexafluoride (SF_6) is used instead of helium to produce cylinders that are roughly five times the

density of the surrounding air. Except for modifications that were needed to accommodate a heavy gas jet, the experimental set-up is unchanged from Part 1. The most important of these modifications is that the heavy gas jet is directed vertically downward, instead of upward, in the shock tube. A brief description of the experimental apparatus is given in the following section. For a more complete description see Part 1 of this series (Jacobs 1990).

2. Experimental Apparatus

Experiments were carried out in a 26.67 cm square test section mounted to the Galcit 17 inch shock tube. A 152.4 cm long "cookie cutter" was used to provide a transition from round shock tube to square test section. Visual access to the test section was provided by a pair of 15.24 cm diameter round windows. 0.152 mm thick aluminum diaphragms were used to produce a shock Mach number of approximately 1.095. A laminar SF_6 jet was introduced into the test section with the same rig used in Part 1. SF_6 is heavier than air, so the rig had to be turned upside down to produce a stable jet. The jet issued from a 0.794 cm diameter opening oriented vertically downward, directly on top of the lower window. Similarly, a larger 1.9 cm opening, was situated 8.9 cm directly below the jet exit, to collect the heavy gas and remove it from the shock tube. The SF_6 supply was split into two streams with one stream passing through a pool of liquid biacetyl seeding it with nearly saturated vapor. A ratio of 6 parts pure SF_6 to 1 part biacetyl laden SF_6 was used with a total flow rate of 11.6 cc/s.

Planar laser induced fluorescence utilized a flashlamp pumped dye laser providing 100 mJ 0.7 μs pulses of 430 nm laser light. The resulting 18 mm beam was focused using a set of lenses to provide a sheet of laser light that bisected the biacetyl seeded SF_6 jet, illuminating a 1 mm thick cross section . The jet/laser sheet orientation is illustrated in figure 1. The resulting fluorescent image was captured using an intensified solid state video camera that was positioned so that it viewed upward through a window in the bottom of the test section. The camera output was sent to a frame grabber housed in a laboratory microcomputer. A shadowgraph system consisting of a spark source, two concave mirrors, two flat mirrors, a video camera and a frame grabber was also

used to visualize the flow. This system was oriented horizontally, so that a view of the full length of the jet could be obtained. Timing was accomplished using digital delay generators, triggered by signals from pressure transducers mounted flush in the test section walls.

In these experiments, biacetyl is used as a tracer for the gas initially contained in a laminar jet. The effectiveness of a tracer, whenever diffusion is occurring, is governed by how closely matched the diffusion of the tracer is to that of the tagged species. In the light gas experiments of Part 1, biacetyl was used as a tracer for helium. It was found that biacetyl and helium have largely different diffusion coefficients. Because of this fact, care had to be taken in interpreting the PLIF results, especially when mixing was an issue. In the present experiments, the diffusivities of SF_6 and biacetyl are much more closely matched. Thus, biacetyl a much better tracer for SF_6, and measured PLIF intensities more closely correspond to SF_6 concentration.

3. Results and Discussion

Shadowgraph was primarily used in these experiments to provide full-length views of the evolving heavy gas cylinder. However, the system was also useful in monitoring the SF_6 jets, to determine what flow rates provided jets of sufficient uniformity. In doing so it was discovered that much lower flow velocities were needed to produce jets free from instabilities, in these experiments, than were required in the previous experiments using helium jets. This is because SF_6 has a much lower kinematic viscosity than helium (0.025 cm^2/s as opposed to 1.22 cm^2/s for helium). Thus, an SF_6 jet with the same velocity as a helium jet has a much higher Reynolds number. A flow rate of 11.6 cc/s was chosen as providing the best results; though, even at this flow rate, instability waves were still present . This gave a jet Reynolds number of 730,.based on the mean velocity. Figure 2a is a shadowgraph photograph of a typical jet. As was found with the helium jets, the magnitude of suction applied to remove the SF_6 stream had no effect on the stability of the jet.

Runs were made utilizing the shadowgraph system to determine whether the flow resulting from a nearly two-dimensional jet remains nearly two-dimensional. All runs in this study were

made at an incident shock Mach number of approximately 1.095. Figures 2b, c and d are photographs taken 0.112, 0.510 and 0.927 ms after the passage of the shock wave. Figure 2b shows the shock wave shortly after having passed through the SF_6 jet. The sequence shows that jet segment is chopped off of its support by the flow behind the shock. Except for small regions confined to the ends of the jet segment, the jet remains remarkably straight.. The jet segment becomes slightly skewed as it is pushed down the shock tube. This effect is a result of a variation in density along the length of the jet caused by the outward diffusion of SF_6. Portions of the jet farther from the jet exit (and thus of slightly lower density) are pushed faster (and thus farther downstream) than sections closer to the exit.

Confident that the flow was very nearly two dimensional, runs were made utilizing laser induced fluorescence to obtain a cross-sectional view of the flow. This cross section was taken 3.81 cm from the jet exit (4.8 jet exit diameters). Figure 3 is a sequence of PLIF images taken from these runs. The pictures are displayed in false color with white representing the lowest fluorescent intensity and yellow the highest. Figure 3 contains images from 8 separate runs, all with nearly identical conditions and taken at different times after the passage shock wave. Also shown is a view of a typical quiescent jet cross section (figure 3a). Note that initial jet cross section is not perfectly circular. This lack of symmetry is most likely caused by an instability of the laminar jet that is too small to be visible in the shadowgraph images. In experimenting with the SF_6 flow rate, it was found that the degree of asymmetry could be decreased (or increased), by decreasing (or increasing) the flow. However, when the flow rate was reduced below 11.6 cc/s, a more disruptive instability developed. Thus, perfectly symmetrical jets could not be obtained. The degree of asymmetry changed daily, even though great care was taken to insure that the test conditions were identical. It is for this reason that it is believed that the asymmetry is a result of an instability.

Figure 3b, taken 0.217 ms after the passage of the shock, shows an initial flattening of the cylinder, caused by the compression of the shock wave, and the beginning of the formation of a crescent shape. The protrusion near the center of the downstream edge of the cylinder in figure 3b

and c is caused by a jet of fluid that is produced by the focusing of the transmitted shock wave. Figure 3c, taken at t = 0.374 ms, shows further spreading of the crescent shape. In figures 3d and e, vorticity that initially resides on the boundary of the cylinder appears to be shed from the heavy gas and collect in the wake of the cylinder to form a vortex pair. The heavy gas strip is then wrapped around these vortices by their induced velocity. Figure 3f shows the beginning of the formation of waves on the heavy gas strip. In figure 3g these waves continue to grow as the gas is swept to the rear of the vortices. In figure 3h, similar waves can be observed in the thin filaments of heavy gas that spiral into the vortex cores. Finally, as the heavy gas builds up at the rearward stagnation point, the waves have grown to a point where they dominate the flow and further help dissipate the gas.

In these experiments, vorticity is produced by the interaction of a plane shock wave with the density gradient at the jet boundary. The magnitude of this vorticity is proportional to the product of the density and pressure gradients as well as to the degree of their misalignment. Thus, the vorticity is localized at the jet boundary, and is distributed such that it is maximum at the cross-stream edges of the jet and zero at the front and back edges. This gives the vorticity the form of two semicircular vortex sheets of opposite sign. The vortex strength distribution in these sheets is maximum at the center of the sheets, and decays to zero at the ends. From this viewpoint, the difference between an accelerated light gas cylinder and a heavy one is in the sign of the vorticity. And to first approximation, one would expect the evolution processes for these two cases to be similar, but having opposite sign. However, the pictures of figure 3 reveal a completely different process than what was observed in the light gas experiments of Part 1. In the light gas experiments, the later stages of development were characterized by a small amount of helium becoming incorporated with the vorticity, and eventually becoming part of the vortex cores. Where as, in the heavy gas experiments shown in figure 3, the bulk of the vorticity separates form the heavy gas to form line vortices that are free from SF_6.

The qualitative differences between these two cases can be explained with the aid of the simple model. In the experiments, circular regions of either a light or heavy gas have vorticity that

is distributed on the boundary. This vorticity is distributed such that it is concentrated on opposite sides of the cylinder. This configuration can be reasonably approximated by the simpler model of a vortex located at the vertex of a wedge shaped region of a gas that is either lighter or heavier than its surroundings. This model is illustrated in figure 4a for a heavy gas wedge and in figure 4c for a light gas wedge. In this configuration the vortex will induce a circular motion around its center, causing the wedge to wrap around its vertex. The resulting centripetal acceleration, caused by the circular motion of the fluid, will produce a radial pressure gradient given by

$$\frac{\partial p}{\partial r} = \rho \frac{v^2}{r}.$$

However, the gases inside and outside the the wedge have different densities, so the gradient will have different values in the two fluids. If the density is larger inside the wedge, the pressure gradient will be larger inside the wedge as well. The pressure is assumed to be uniform at infinity (where there is no motion). Thus, the pressure will be lower inside the wedge near the vortex, and there will be a pressure difference across the interface separating the two gasses. This pressure difference will produce a secondary motion causing the interface to move inward, pinching off the vertex of the wedge as shown in figure 4b. Now if the wedge shaped region contains gas that is lighter than its surroundings, the process is reversed. The pressure gradient would be smaller inside the wedge, resulting in higher pressure inside than out. This would produce a secondary flow causing the interface to move outward, and the wedge would swell as shown in figure 4d. Thus with a heavy gas wedge, the vortex is pinched off from the heavy gas, promoting separation. With a light gas, the wedge swells, encompassing the vortex. These results can be viewed in another way. The circular motion induced by the vortex produces centrifugal forces. These forces operate on the surrounding fluid by forcing the heavier of the two gases away from the vortex. At the same time, continuity ensures that the lighter of the two gases moves toward the vortex. Thus, lighter gases are attracted toward vorticity, and heavier gases are repelled.

This process is further enhanced by the differences in the rates of the diffusion of vorticity in the two gases. Suppose a uniform distribution of vorticity were deposited on the boundary separating two quiescent gases having different kinematic viscosities. Since the rate at which vorticity diffuses in a fluid is governed by its kinematic viscosity, the vorticity will diffuse much more readily into the more viscous gas. After a period of time, more of the original vorticity would reside in the more viscous gas than in the less viscous one. The kinematic viscosity of a gas is closely linked to its density. Heavy gases almost always have lower kinematic viscosities than lighter ones. Thus, in cases with largely different density, vorticity will tend to diffuse into the lighter gas and away from the heavier one. This process together with the dynamic mechanism described above explains why the vorticity, originally deposited on the cylinder boundary, eventually ends up in the lighter of the two gases.

The latter half of the evolution process shown in figure 3 is dominated by the growth of a disturbance on the deforming heavy gas cylinder. The disturbance is initially of small amplitude, however it soon grows to a point where it drowns out the original features of the flow. This type of behavior indicative of an instability. At the point of first appearance, waves arise on a strip of a heavy gas that is being wrapped around a vortex pair. This wrapping cannot be accomplished without a sizeable centripetal acceleration. Thus the heavy gas strip resides in a very strong acceleration field. In this configuration the strip is susceptible to Rayleigh-Taylor instability. A second cause for instability may result from shear. Most of the vorticity that was initially deposited on the heavy gas cylinder by the passing shock wave is shed by the heavy gas. However, it is very likely that a small amount of vorticity still resides at the edge of the heavy gas at the point where the waves begin to form. Thus, the heavy gas strip is in a shear flow and is likely to experience Kelvin-Helmholtz instability. The growth of the disturbances observed in the PLIF images is probably a result of both mechanisms described above. At the point when the disturbance first appears the instability is in an accelerated shear flow. Thus, the instability results from a combination of Rayleigh-Taylor and Kelvin-Helmholtz instabilities.

A remarkable result of the light gas experiments in Part 1 was the symmetry of the cross-sectional views of the deforming helium cylinder. In viewing the sequence of figure 3 it is clear that this degree symmetry is not shared with the current experiments. Even though the images in figure 3g-i appear to be chaotic, the general features of the flow observed in figure 3 were very repeatable. Slight daily variations *did* exist in these experiments. However, these differences were mainly in the degree and time of appearance of the instability. For instance, the time that the instability waves first appeared on the heavy gas strip differed from day to day. However, the instabilities always appeared first (and grew to a greater degree) on the side of the cylinder corresponding to the top of photographs in figure 3. It is believed that these instabilities were a direct result of the nonuniformity present in the initial laminar jet. The size and time of appearance of these disturbances were dependent on the degree of initial nonuniformity. Thus, the asymmetrical flow pattern observed in figure 3 was a direct result of asymmetries in the initial state.

3.1 Displacement

A shock wave traveling down the shock tube will accelerate a fluid particle that it travels through, from rest to a constant velocity V where

$$V = \frac{2a_0}{\gamma + 1}\left(M_s - \frac{1}{M_s}\right)$$

Here γ is the ratio of specific heats and a_0 is the speed of sound preceding the shock. The shock wave will similarly accelerate a fluid particle residing in the jet, but because SF_6 is heavier than air, the heavier gas will be accelerated to a velocity less than V. Thus the cylinder travels downstream more slowly than the surrounding gas. For a very short period of time the SF_6 cylinder translates through the air as though it were solid. However, the cylinder very rapidly is forced to deform, and eventually becomes wrapped around a vortex pair. Figure 5 is a plot of the downstream

displacement of the cylinder (X) relative to the displacement of an air particle behind the shock wave (Vt), scaled by the jet exit diameter (D). The location of the cylinder was found by taking the center of area of all pixels that were brighter than one half the maximum pixel brightness in each image. Time is scaled in this plot by the length of time it takes a free stream particle to travel one jet exit diameter (D/V). The data of figure 5 indicate that the cylinder initially travels at its greatest (negative) velocity and that this velocity continuously decays with time. Note that this velocity is relative to the free stream, so that a negative velocity simply means that the cylinder is traveling downstream at a rate less than the surrounding gas. Thus, in the laboratory frame of reference, the cylinder initially travels at its slowest velocity and is continually accelerating as time progresses. Also note that, early on, the data fall nicely on a single trajectory with very little scatter. However, halfway in the evolution process, the scatter increases dramatically. The point where the scatter suddenly increases corresponds with the point where instability waves appear on the heavy gas strip. The appearance of waves on the heavy gas strip would very likely increase the drag of the distorted cylinder, and thus cause a sharp reduction in the relative velocity. It was mentioned earlier that the time of appearance of the waves varied from run to run. This variation coupled with the increased drag caused by the instability waves would account for the inconsistencies or scatter in the trajectory of figure 5

Rudinger & Somers (1960) gave a simple analysis to describe the displacement of a shock accelerated gas volumes, and found two asymptotic values of translational velocity. In the first, they assumed that the inhomogeneity initially behaved like a solid cylinder accelerated by a passing shock wave. In the second they assumed that, after a sufficient period of time, the motion was that of a vortex pair with the hydrodynamic impulse and circulation of an infinite lamina accelerated from rest. The first velocity (here computed relative to the surrounding gas) is given by

$$U_i = \frac{1-\sigma}{1+\sigma} V, \qquad (1)$$

and is asymptotically valid for small times. The second velocity is given by

$$U_f = \frac{2}{\pi^2} U_i, \tag{2}$$

and is asymptotically valid for large times. Here σ is the ratio of cylinder to surrounding gas density, which for a SF_6/air system equals 5. Substituting this value into equations 1 and 2 gives $U_i = -0.67V$ and $U_f = -0.14V$. Note that this analysis is appropriate for small flow Mach numbers (V/a_0), and large Reynolds numbers.

Figure 6 is a plot similar to figure 5 showing the displacement of the cylinder center of area along with the displacement of the vortex cores. Also drawn on this plot are two lines with slopes equal to the velocities that are obtained using equations 1 and 2. The agreement between the initial velocity (equation 1) and the data is reasonably good; although the theory slightly underpredicts the data. When the final velocity (equation 2) is compared with the vortex pair displacement, it is found that the theory significantly underpredicts the vortex pair velocity. Figure 7 is a plot of the vortex spacing (d) shown scaled with jet exit diameter (D). The plot shows that the spacing remains remarkably constant throughout the evolution process, and that the spacing ratio is approximately equal to 1.4. This ratio is significantly greater than that given by the theory of Rudinger & Somers (1960) ($d/D = \pi/4$).

The velocities from the theory of Rudinger & Somers (1960) were calculated assuming the jet core contained pure SF_6. In the experiments, the heavy gas is steadily diffusing out of the jet as it crosses the test section. Thus, the actual jet density is slightly lower than that of pure SF_6. However, a lower density ratio in equations 1 and 2 would give smaller values for both the initial and final velocities. Thus, this effect cannot explain the discrepancy between equation 2 and the measured vortex displacements. The discrepancies between experiment and theory are more likely caused by the limited ability of the simple model used by Rudinger & Somers to describe the flow that is observed in figure 3. For instance, the model assumes that after sufficient time, the flow is described by a vortex pair with strength given by the initial flow field. However, the final flow

field is computed assuming uniform density. The presence of a gas strip that is five times the density of air, wrapped around this vortex pair, certainly has some effect on the flow field. This effect, however, is not accounted for in the model.

Haas & Sturtevant (1987) measured the downstream velocities of several notable points on the interface separating the two gases. These included the upstream and downstream edges of the part of the deforming cylinder that intersects the symmetry plane, and the downstream edge of the vortex. The downstream displacements of these particular points were measured in the present experiments and are shown plotted in figure 8. Also shown in figure 8 are the downstream displacements of the center of area, and of the vortex cores. The initial and final velocities of these points were measured by fitting appropriate portions of the data using linear regression. These curve fits are shown on figure 8 plotted as solid lines. The measured velocities obtained from these fits (which are relative to the velocity of a fluid particle at infinity, V) are listed in table 1. In addition to velocities measured in the present experiments, table 1 contains values obtained under similar conditions by Haas & Sturtevant (1987) and by Picone & Boris (1988), as well as results from the theory of Rudinger & Somers (1960). Note that the results of Haas & Sturtevant and Picone & Boris were obtained using a gas having a smaller density ratio (σ) than the one used here. Thus, the present measurements are noticeably larger (i.e. more negative). Considering this difference, the agreement between the present experiments and the earlier work is reasonable. Also note that the velocity of the vortex downstream edge reported by previous authors differs considerably from the present measurements. These unusual values were caused by wall effects which influenced the previous work and are absent here.

3.2 Mixing

In Part 1 of this series, the decrease in cross-sectional area of the deforming helium cylinder was used as a gauge of the rate of mixing. In the current experiments, these cross-sectional areas were similarly measured. Figure 9 is a plot of these areas, scaled with the initial jet area. This data was computed by finding the area of the portion of the deformed cylinder that is

brighter than one half the brightest point in that particular image. The data of figure 9 show a gradual decline in the cross-sectional area during time spanned by these experiments. It is apparent that this decrease occurs not nearly as rapidly as was measured in the light gas experiments of Part 1. The decrease of cross-sectional area was thought to be a reasonable diagnostic in Part 1, primarily because it was found that the the maximum concentration did not significantly change in the process. Figure 10 is a plot of the maximum biacetyl concentration for the current experiments. This data is noisy and sparse, however it clearly shows a decrease in the maximum concentration with time. Since the maximum concentration is not constant in the current experiments, the decrease of cross-sectional area is not a good diagnostic for mixing. Since the concentration decreases with time, a combination of cross-sectional area and concentration must be used.

Figure 10 shows that the decrease in concentration occurs slowly at first, increasing toward the end of a run. This fact in combination with the data of figure 9 implies that the heavy gas cylinder mixes more slowly at first, then increases later on. In viewing the PLIF images, it was observed that the heavy gas separates from the vorticity, early in the evolution process. Vorticity is the source of the high strain rates that promote mixing in this flow. Furthermore, the magnitude of this strain rate diminishes with distance from the source. Thus, the farther a region is from the vorticity, the more slowly it is mixed. One would then expect the mixing of a heavy gas cylinder to (at least initially) proceed at a slower rate than for a lighter gas one. Figure 10 shows that the concentration decreases markedly toward the end of the plot. This corresponds to the stage where the heavy gas has collected at the rear of the vortex pair. At this point the mixing proceeds at a much faster rate. However, it is difficult to say whether this rate is greater than that of the light gas case.

4. Conclusions

Experiments were carried out in which a cylindrical volume of a heavy gas was impulsively accelerated by weak shock waves. A laminar jet of SF_6 was used to produce the heavy gas cylinders. Planar laser induced fluorescence and shadowgraph were used to visualize the flow. It

was found that, unlike the light gas case, vorticity separates from the heavy gas early in the evolution process. A simple model which explains these differences was presented. The model shows that centripetal acceleration is the cause of these differences. Centrifugal forces cause light gasses to be attracted to the vorticity, while at the same time these forces cause heavy gasses to be repelled. This process is enhanced by the different rates of the diffusion of vorticity in the two gases, caused by large differences in kinematic viscosity. It was also found that the latter stages of the evolution process were dominated by the growth of an apparent instability. This instability first emerges as waves on the heavy gas strip that gets wrapped around the vortex pair. These waves soon grow to a point where they dominate the flow. It is believed that this instability is a result of a combination of Rayleigh-Taylor and Kelvin-Helmholtz instabilities.

The downstream displacement of the evolving heavy gas cylinder was measured and compared with the theory of Rudinger & Somers (1960). The agreement between experiment and theory was found to be good, initially. However, the theory significantly underpredicts the final vortex pair velocity. The spacing of the vortex cores in these experiments was also measured. It was found that this spacing remains remarkably constant, and is significantly larger than that indicated by theory. The cause for this differences may be the effect of viscosity (or Reynolds number). However, the simple model used in the theory cannot account for the effects of nonuniform density on the flow. Finally, the downstream velocities of several notable points on the SF_6/air interface were measured and compared to the experimental values of Haas & Sturtevant (1987), as well as to the computational values of Picone & Boris (1988). The present measurements agree reasonably well with the others, considering that the previous results were obtained using a gas with a slightly lower density.

Cross-sectional areas of the SF_6 cylinders were computed as it was done in Part 1. It was found that these areas decrease at a rate significantly less than that of the helium cylinders. However, it was also found that the maximum biacetyl concentration decreases at the same time. Thus, the decrease of cross-sectional area is not a valid diagnostic for mixing in this case. It appears that mixing occurs initially more slowly for the heavy gas cylinder. This is a logical

outcome since it was found that most of the vorticity separates from the heavy gas, thus decreasing its ability to mix. It also appears that the mixing rate increases late in the run, probably as a result of the growth of instability waves. However, it is not clear whether this final rate is greater than that of the helium cylinders.

Acknowledgments

The author wishes to thank Professors F.E. Marble, E.E. Zukoski and B. Sturtevant for their help and support with this research. Credit is due to Dr. R. Miake-Lye for his help with laser induced fluorescence system. Professor C.H.K. Williamson also deserves credit for his helpful comments and suggestions during the preparation of this paper. This work was supported by the Air Force Office of Scientific Research contract F49620-C-0113.

References

Epstein, A.H. 1977 Quantitative density visualization on a transonic compressor rotor. *J. Engineering for Power, Trans. ASME* **99**, 460-475.

Haas, J.-F. & Sturtevant, B. 1987 Interaction of weak shock waves with cylindrical and spherical gas inhomogeneities. *J. Fluid Mech.* **181**, 41-76.

Jacobs, J.W. 1990 Shock accelerated cylindrical gas inhomogeneities Part 1. Shock induced mixing of a light gas cylinder. submitted to *J. Fluid Mech.*

Meshkov, Y.Y. 1969 Instability of the interface of two gases accelerated by a shock wave. *Izv. Akad. Nauk. SSSR Mekh. Zhidk. Gaza.* **4**, 151-157.

Picone, J.M. & Boris, J.P. 1988 Vorticity generation by shock propagation through bubbles in a gas. *J. Fluid Mech.* **189**, 23-51.

Richtmyer, R.D. 1960 Taylor instability in shock acceleration of compressible fluids. *Commun. Pure Appl Maths* **23**, 297-319.

Rudinger, G. & Somers, L.M. 1960 Behavior of small regions of different gases carried in accelerated gas flows. *J. Fluid Mech.* **7**, 161-176.

Table 1. A comaparison of some measured and computed normalized relative cylinder velocities, $\frac{dX/dt - V}{V}$

		Present (σ=5.0)	Haas & Sturtevant (σ=3.6)		Picone & Boris (σ=3.6)	Rudinger & Somers
		M_S=1.095	M_S=1.085	M_S=1.22	M_S=1.22	(σ=5.0)
Upstream edge	Initial	-0.54	-0.10	-0.37	-0.41	--
	Final	-0.31	-0.25	-0.22	-0.21	--
Downstream edge	Initial	-0.65	-0.25	-0.32	-0.43	--
	Final	-0.37	-0.25	-0.32	--	--
Vortex downstream edge		-0.13	0.15*	0.13*	0.13*	--
Center of area	Initial	-0.58	--	--	--	-0.67
Vortex center		-0.26	--	--	-0.15	-0.14

* These values are caused by wall effects

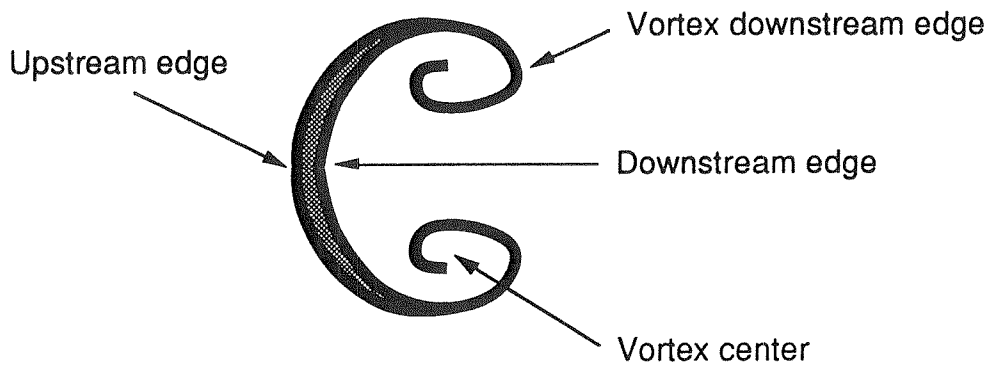

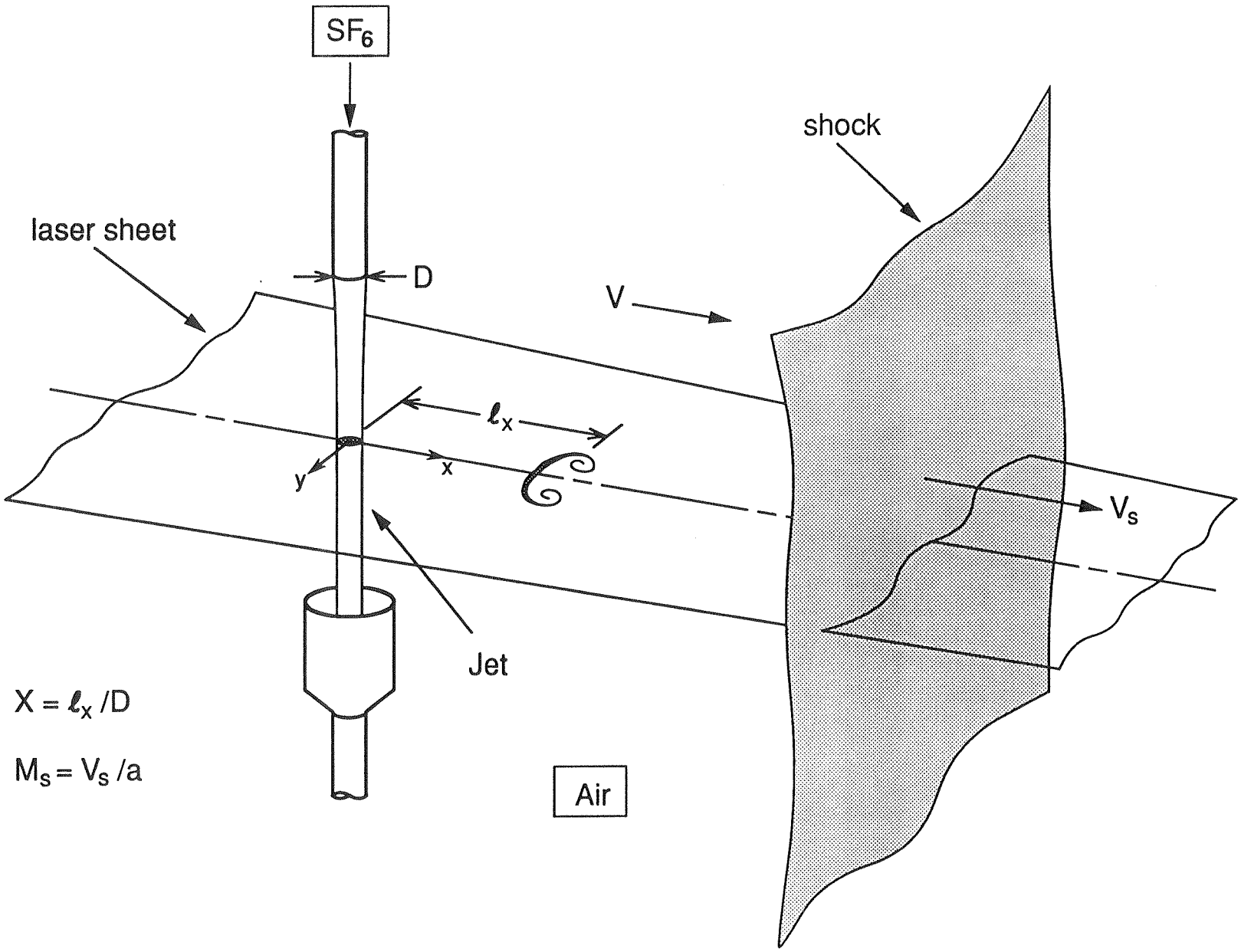

Figure 1. Drawing of the jet/PLIF configuration.

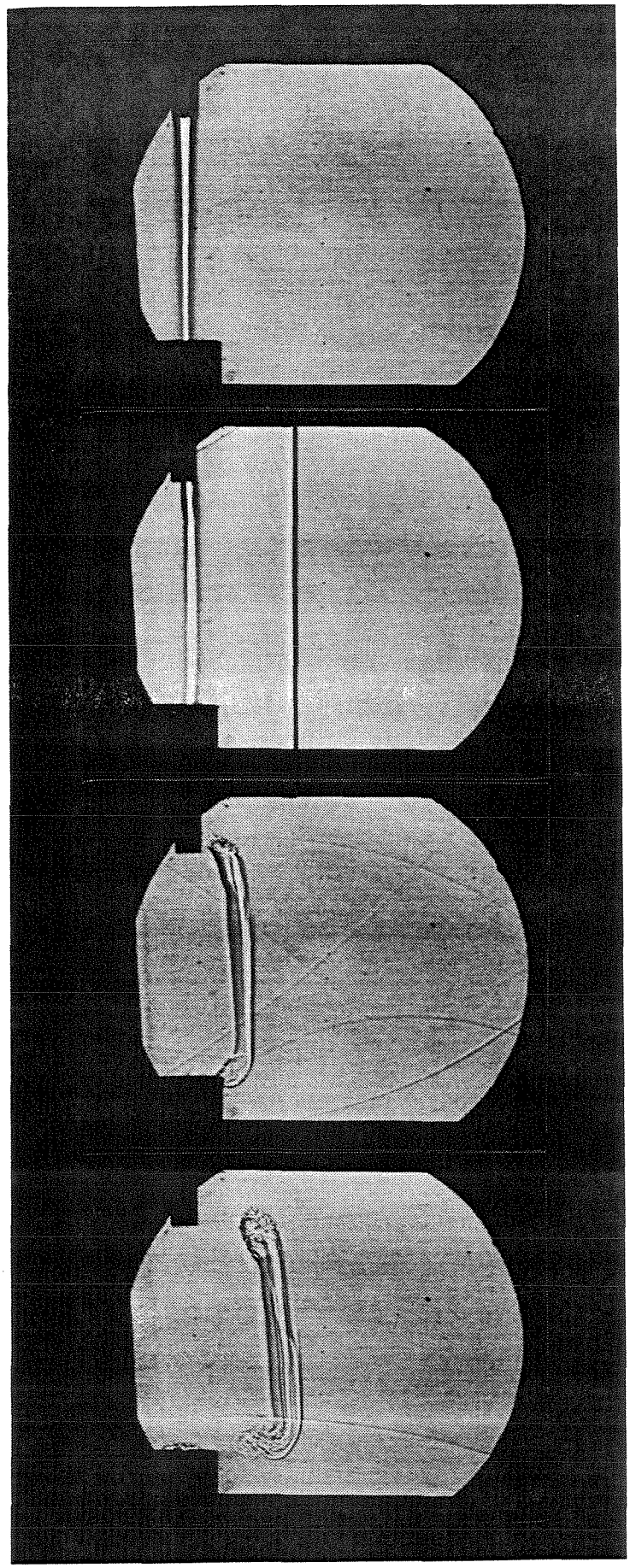

Figure 2. A sequence of spark shadowgraph images giving a side view of the evolving SF6 cylinder. a) The initial jet, b) t = 0.112 ms after the passage of the shock wave, c) t = 0.510 ms, d) t = 927 ms. The Ms = 1.095 shock wave has passed from left to right and is shown in the second photograph after having passed over the heavy gas jet.

Figure 3. A sequence of PLIF images giving a cross-sectional view of the evolving SF6 cylinder. a) The initial jet, b) t = 0.217 ms after the passage of the shock, c) t = 0.374 ms, d) t = 0.588 ms, e) t = 0.803 ms, f) t = 0.998 ms, g) t = 1.201 ms, h) t = 1.403 ms, i) t = 1.803 ms. The Ms = 1.095 shock wave has passed from left to right. The images are from 8 separate runs and were taken at a cross section 3.81 cm from the jet exit.

(Attached)

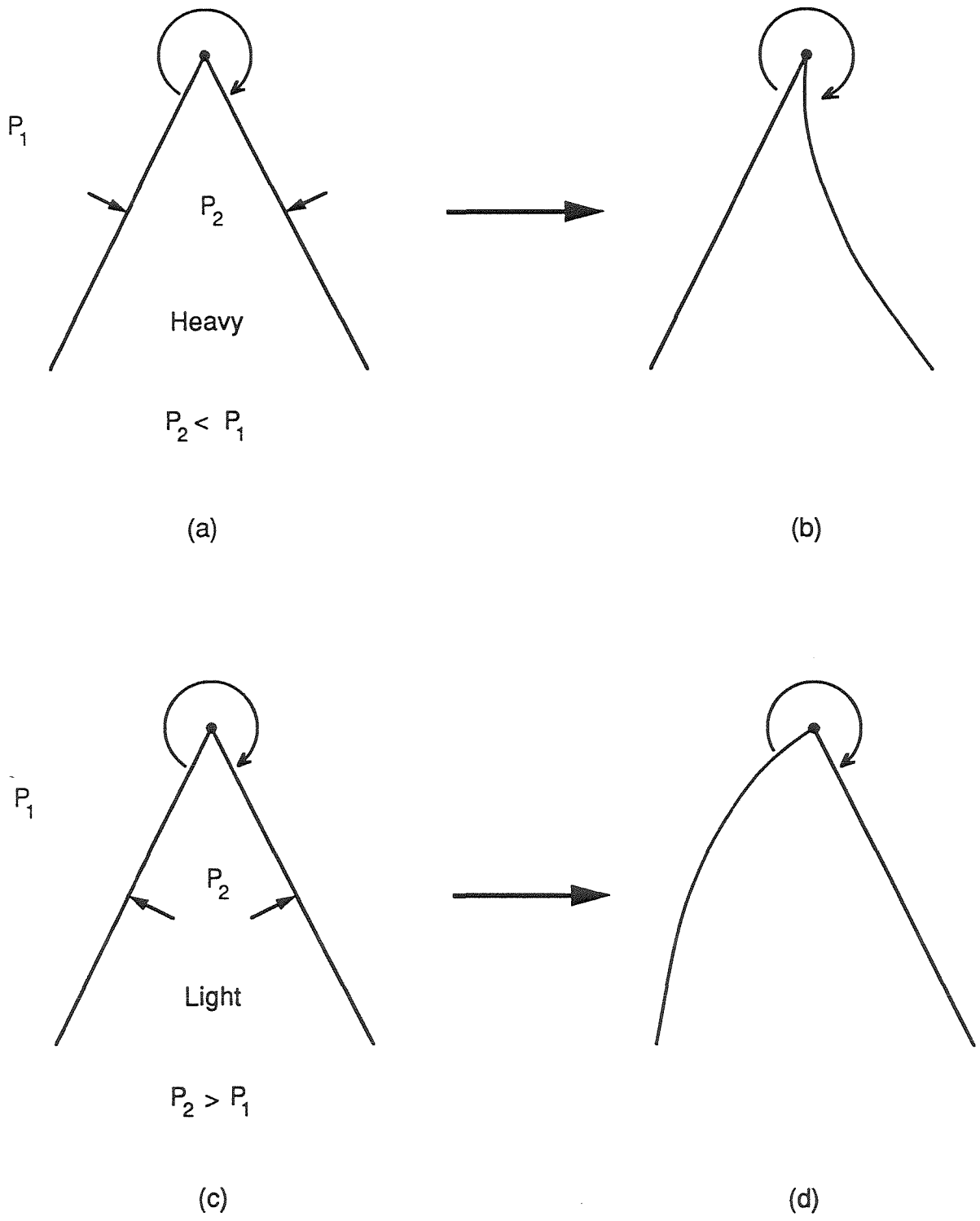

Figure 4. A simple model roughly approximating one side of a shock accelerated light or heavy gas cylinder. a) The heavy gas configuration and b) the resulting motion. c) The light gas configuration and d) the resulting motion.

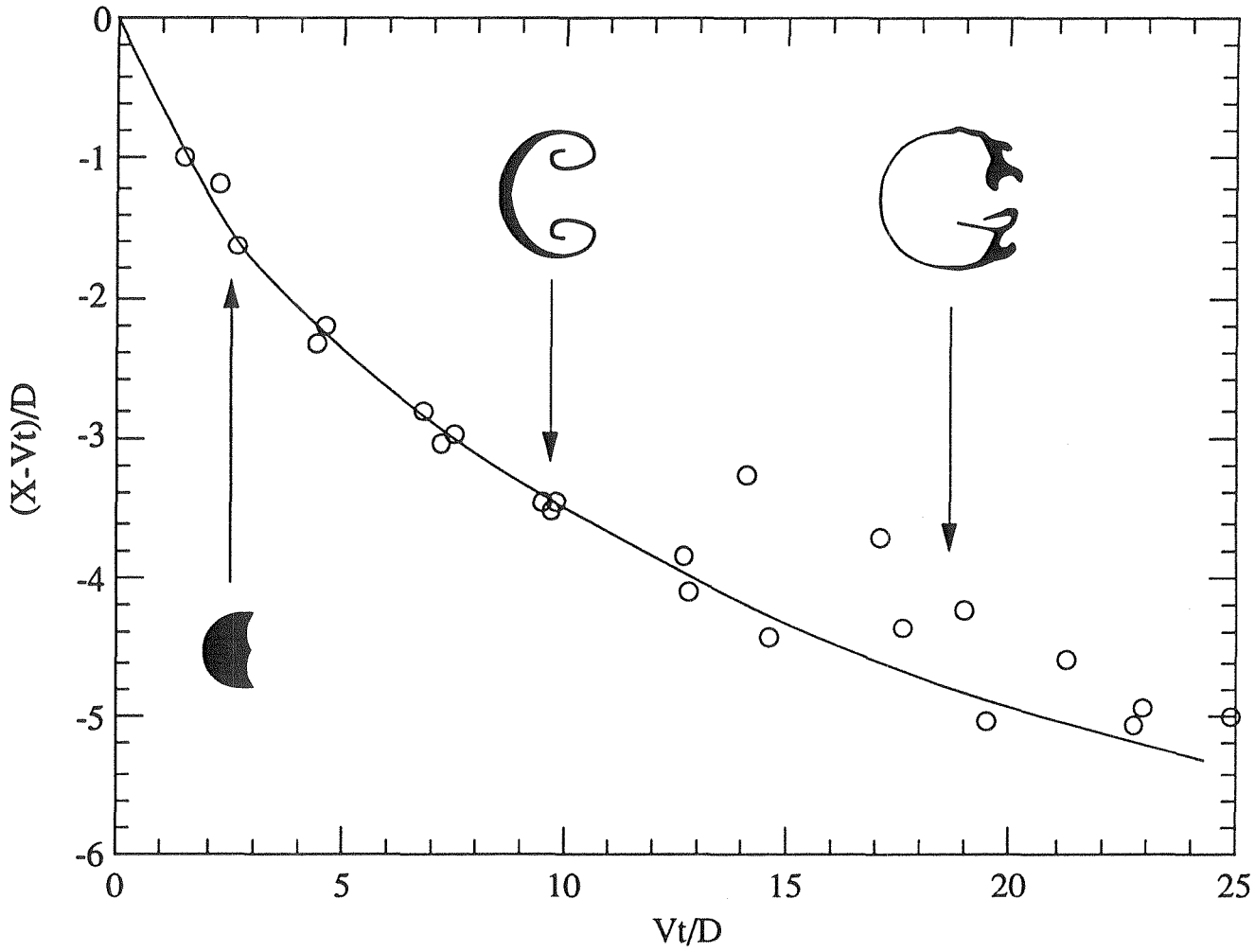

Figure 5. The displacement of the center of cross-sectional area of the SF6 cylinder relative to the free stream.

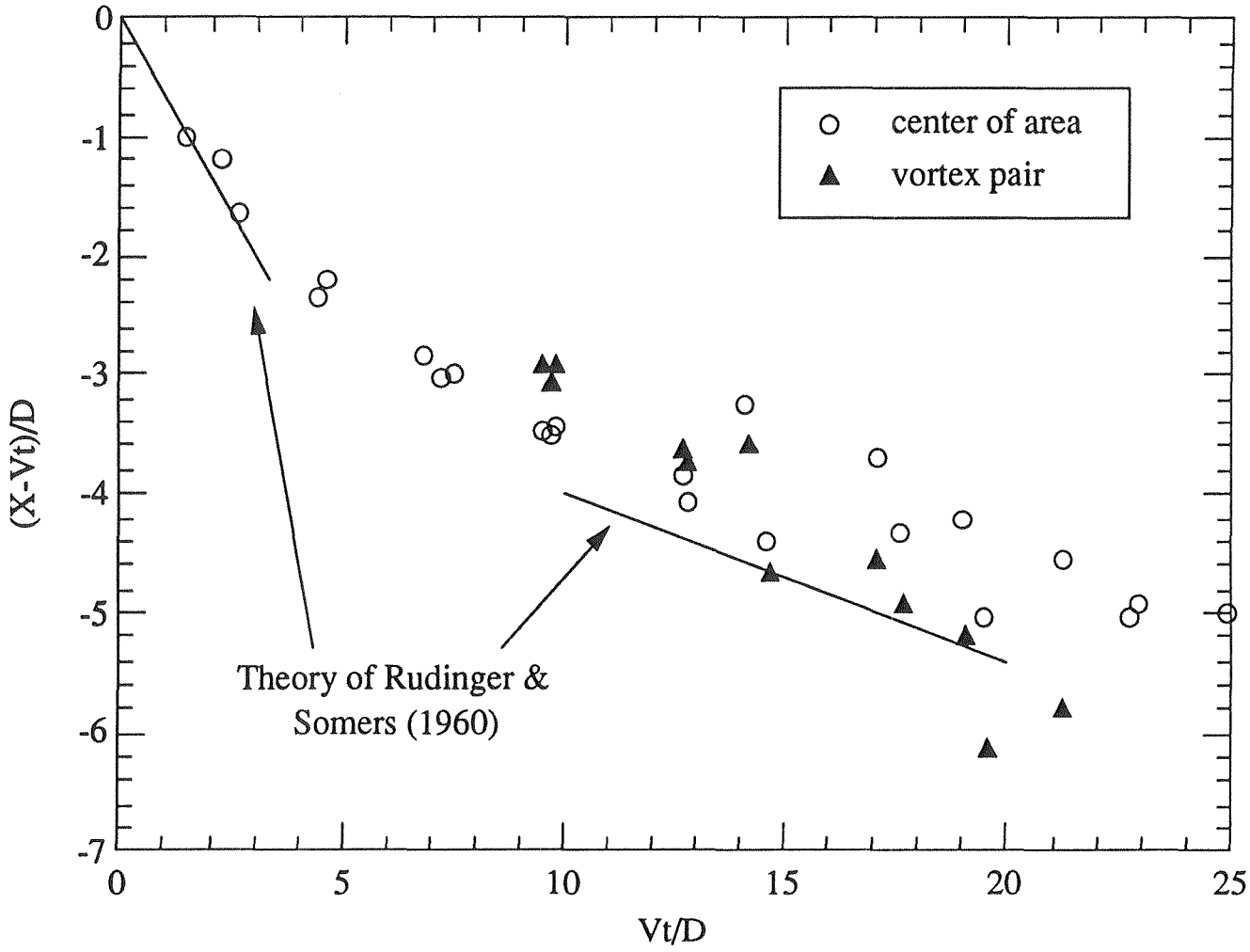

Figure 6. The displacement of the center of cross-sectional area and of the vortex cores relative to the free stream. The solid lines represent velocities obtained using equations 1 and 2.

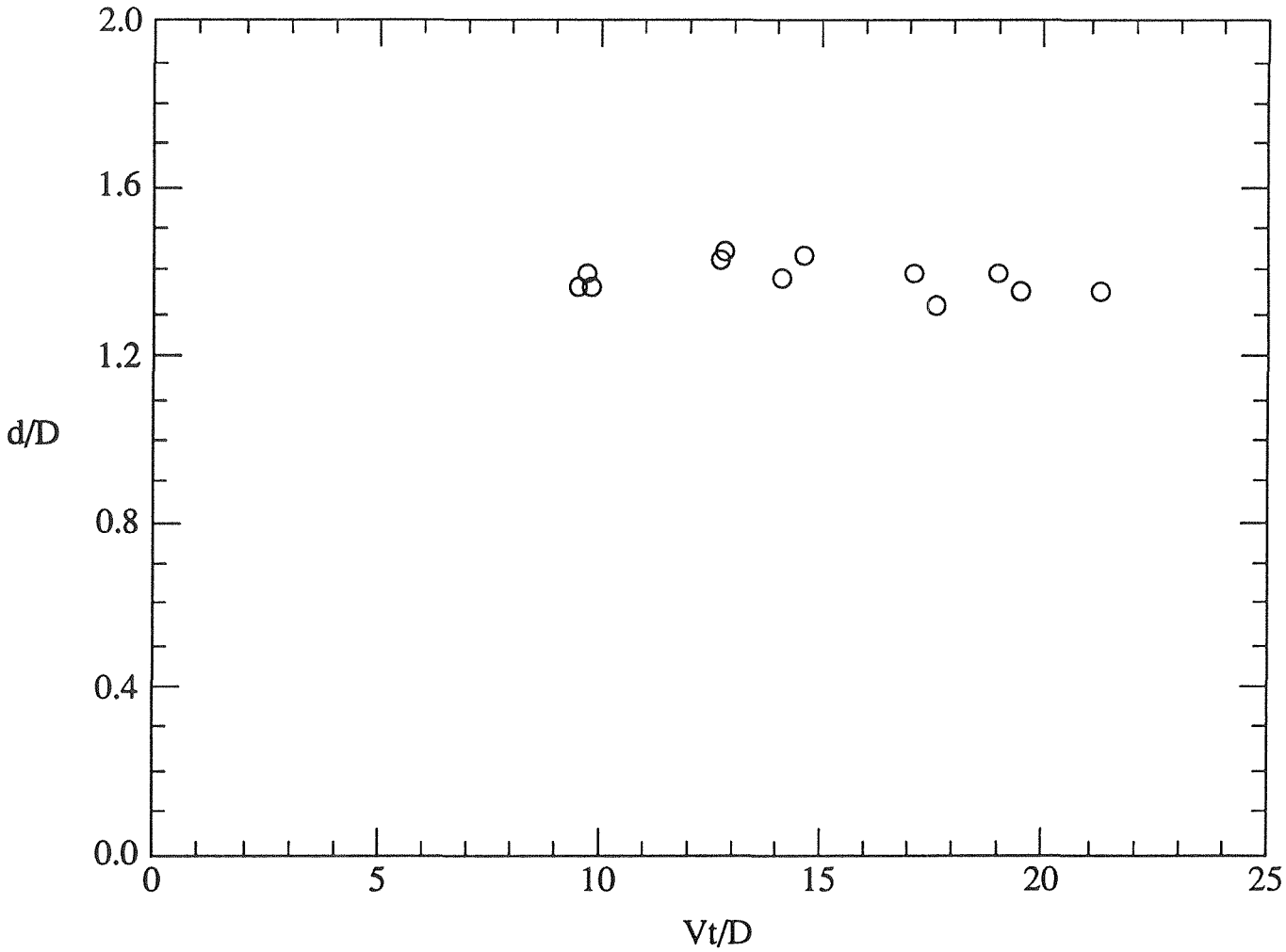

Figure 7. The time evolution of vortex spacing.

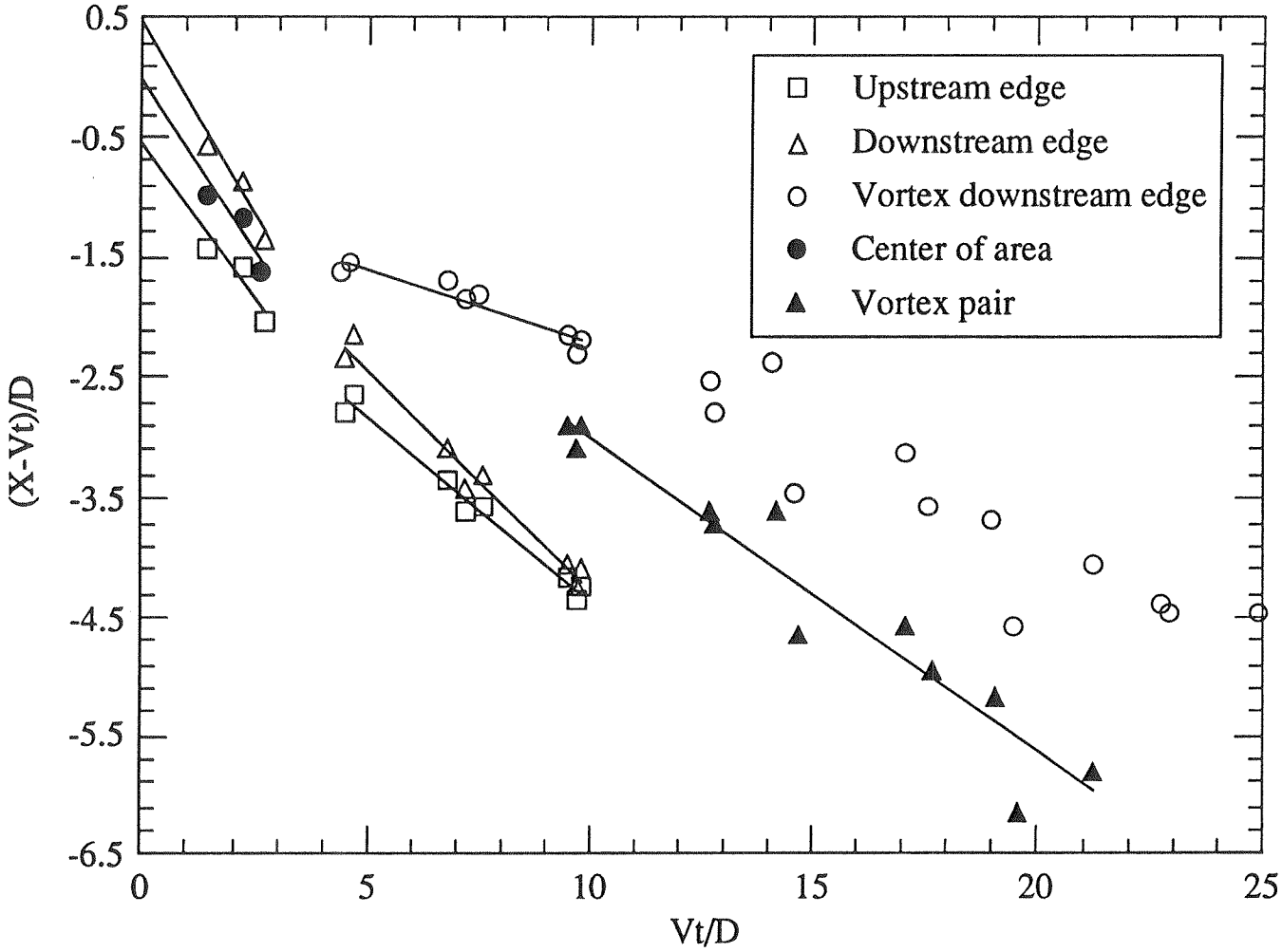

Figure 8. The displacement of various points on the surface of the evolving SF6 cylinder.

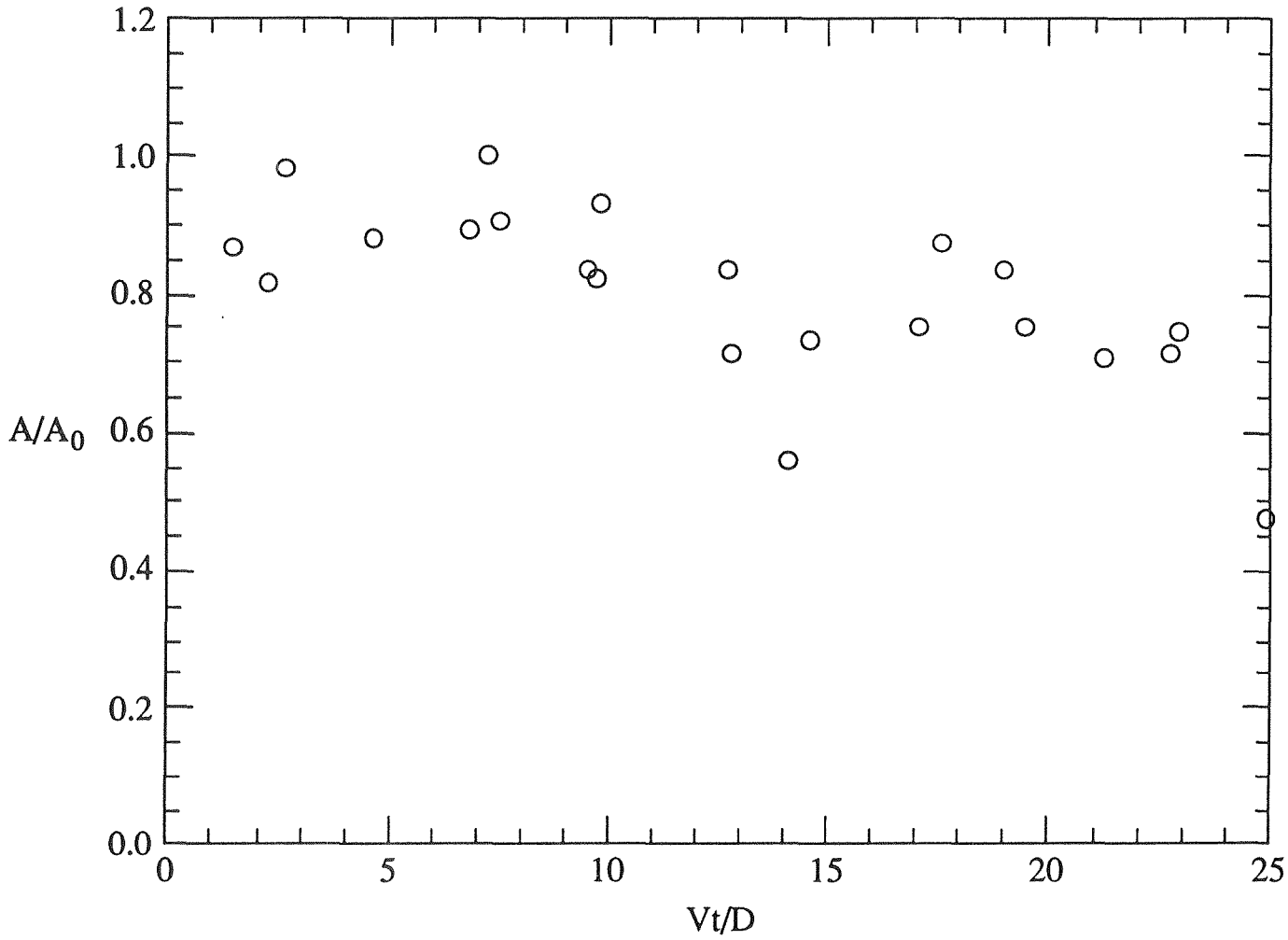

Figure 9. The time evolution of cross-sectional area.

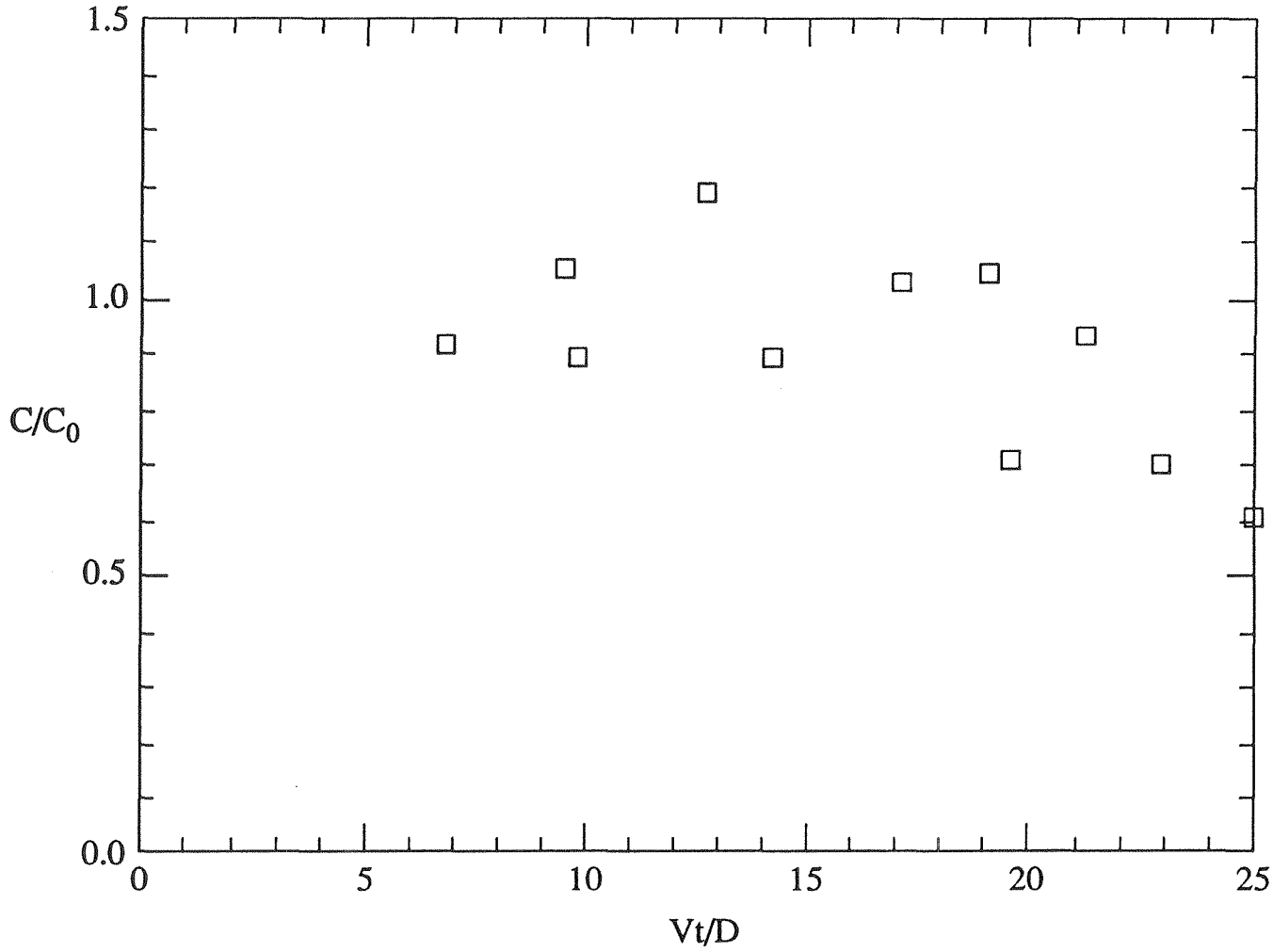

Figure 10. Core biacetyl concentration versus time.

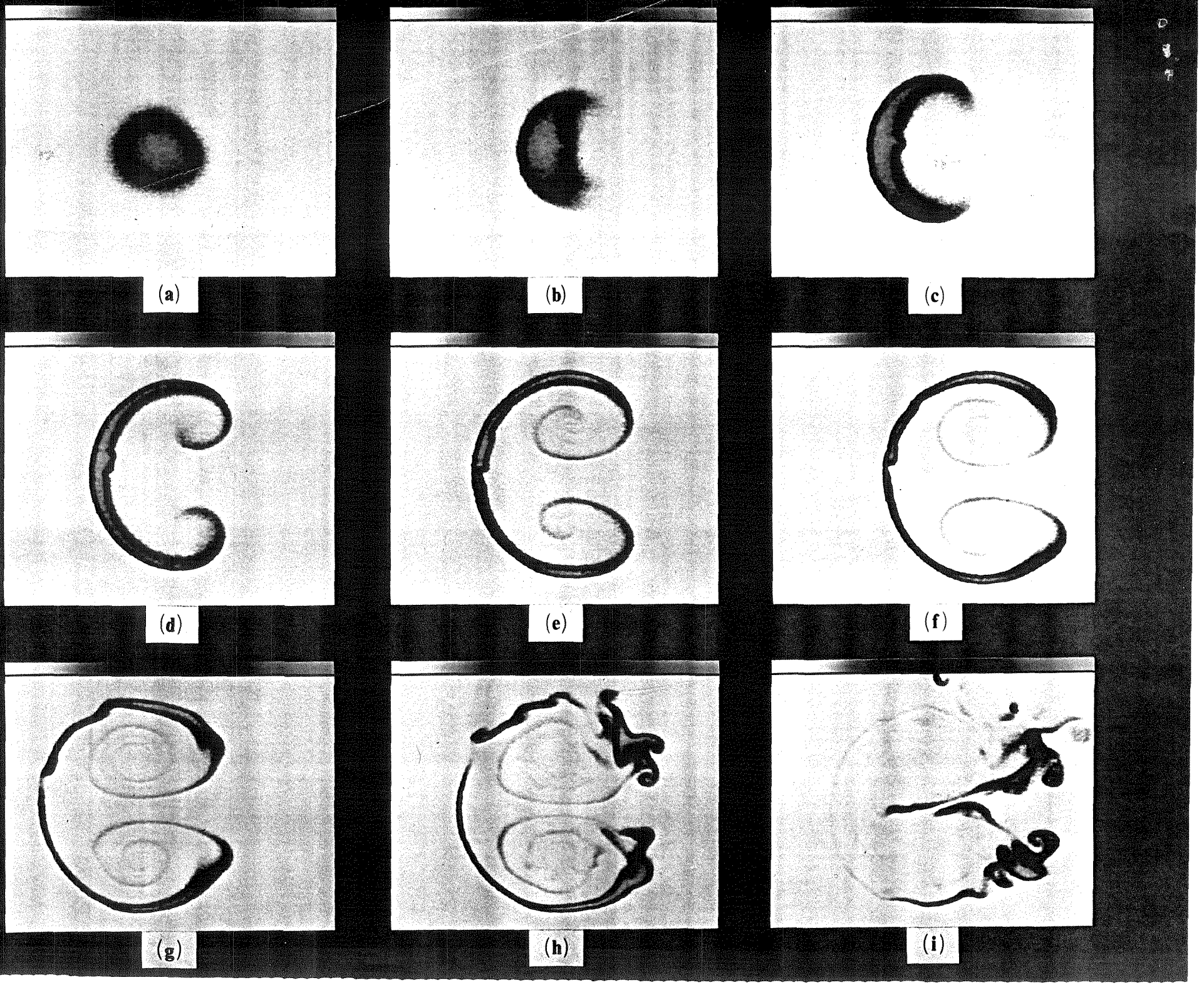
(a)
(b)
(c)
(d)
(e)
(f)
(g)
(h)
(i)